SCISPACE
formerly Typeset

Open access • Journal Article • DOI:10.1063/1.1410388

Covalent attachment of acetonitrile on Si(100) through Si–C and Si–N linkages

— Source link

Franklin Feng Tao, Zhong Hai Wang, Minghua Qiao, Qin Liu ...+2 more authors

Published on: 26 Oct 2001 - Journal of Chemical Physics (American Institute of Physics)

Topics: Thermal desorption spectroscopy, X-ray photoelectron spectroscopy, Chemisorption, Desorption and Acetonitrile

Related papers:

- Controlled molecular adsorption on silicon: laying a foundation for molecular devices.
- Cycloaddition chemistry of organic molecules with semiconductor surfaces.
- A New Opportunity in Silicon-Based Microelectronics
- Organic functionalization of group IV semiconductor surfaces: principles, examples, applications, and prospects
- Cycloaddition reactions of unsaturated hydrocarbons on the Si(100)-(2×1) surface: theoretical predictions

Share this paper:

View more about this paper here: https://typeset.io/papers/covalent-attachment-of-acetonitrile-on-si-100-through-si-c-1zi4v2cyft

Covalent attachment of acetonitrile on Si(100) through Si–C and Si–N linkages

Feng Tao, Zhong Hai Wang, Ming Hua Qiao, Qin Liu, Wee Sun Sim, and Guo Qin Xu

Citation: The Journal of Chemical Physics **115**, 8563 (2001); doi: 10.1063/1.1410388
View online: http://dx.doi.org/10.1063/1.1410388
View Table of Contents: http://scitation.aip.org/content/aip/journal/jcp/115/18?ver=pdfcov
Published by the AIP Publishing

Articles you may be interested in

1,2-Dibromoethane on Cu(100): Bonding structure and transformation to C2H4
J. Chem. Phys. **135**, 064706 (2011); 10.1063/1.3624348

Adsorption and reactions of tetrabutoxysilane (TBOS) on Si(100)
J. Vac. Sci. Technol. A **23**, 613 (2005); 10.1116/1.1927106

Thermal and electron-driven chemistry of CCl 4 on clean and hydrogen precovered Si(100)
J. Vac. Sci. Technol. A **16**, 2995 (1998); 10.1116/1.581451

Thermal chemistry of biacetyl on Si(100)
J. Vac. Sci. Technol. A **16**, 123 (1998); 10.1116/1.580958

Thermal decomposition reactions of acetaldehyde and acetone on Si(100)
J. Vac. Sci. Technol. A **15**, 1146 (1997); 10.1116/1.580445

This article is copyrighted as indicated in the article. Reuse of AIP content is subject to the terms at: http://scitation.aip.org/termsconditions. Downloaded to IP: 129.237.46.99 On: Fri, 20 Nov 2015 20:22:00

Covalent attachment of acetonitrile on Si(100) through Si–C and Si–N linkages

Feng Tao and Zhong Hai Wang
Department of Chemistry, National University of Singapore, 10 Kent Ridge, Singapore 119260

Ming Hua Qiao and Qin Liu
Department of Chemistry, National University of Singapore, 10 Kent Ridge, Singapore 119260, and Department of Chemistry, Fudan University, Shanghai, People's Republic of China 200433

Wee Sun Sim and Guo Qin Xu[a)]
Department of Chemistry, National University of Singapore, 10 Kent Ridge, Singapore 119260

(Received 4 June 2001; accepted 22 August 2001)

The covalent binding and adsorption states of acetonitrile on Si(100) have been investigated using temperature programmed desorption (TPD), x-ray photoelectron spectroscopy (XPS), high-resolution electron energy loss spectroscopy (HREELS), and density function theory (DFT) calculation. XPS and HREELS results show that acetonitrile chemisorbs on Si(100) in a side-on di-σ binding configuration, forming Si–C and Si–N σ bonds. TPD measurements reveal the presence of two desorption states, $\beta 1$ and $\beta 2$ with desorption energies of 29.8 and 24.6 kcal mol^{-1}, respectively. Based on DFT calculations, the $\beta 1$ state is possibly assigned to di-σ bonded acetonitrile on top of a dimer and/or in an in-row bridging chemisorption, while the $\beta 2$ state is related to acetonitrile bonded in a cross-row bridging configuration. © *2001 American Institute of Physics.* [DOI: 10.1063/1.1410388]

I. INTRODUCTION

The scientific and technological development related to silicon-based microelectronics and biosensors is the main driving force for intense research in surface chemistry of organic molecules on Si surfaces.[1] The reactivity of organic molecules on Si(100) is intimately connected with the geometric and electronic structures of the surface Si atoms. The truncation of the diamondlike bulk structure along the (001) direction of silicon crystal leaves each surface Si atom with two σ bonds to the bulk and two dangling bonds with one lone electron in each. The (2×1) surface reconstruction obtained by a simple lateral translation of surface Si-atoms to form Si dimers was first suggested by Schlier and Farnsworth[2] in 1959 and further confirmed in the scanning tunneling microscopic (STM) studies by Hamers *et al.*[3–5]

Many of the physical and chemical properties of Si(100) can be rationalized by considering a double bond feature of dimer, that is, a strong σ bond linking the two Si atoms and a rather weak π bond. All studies of simple alkenes on Si(100) have shown a facial $[2+2]$ cycloaddition reaction pathway;[6–22] despite the fact that, according to Woodward's rule, the analogous reaction of two organic alkenes is forbidden in the high-symmetry suprafacial–suprafacial $[2\pi_s+2\pi_s]$ approach.[23] Moreover, experimental evidence has shown that the molecular stereochemistry is preserved through this reaction, thereby ruling out the suprafacial–antarafacial $[2\pi_s+2\pi_a]$ mechanism.[23]

In order to further understand the reaction mechanism, Hamers *et al.*[24,25] and Bent *et al.*[26,27] extensively investigated the cycloaddition reaction mechanism of cyclopentene and other unsaturated hydrocarbons on Si(100), Ge(100), and C(100). The reactivity of cyclopentene was found to be very different on these three crystals. The reactive sticking probability is approximately unity on Si(100), 0.1 on Ge(100), and $\sim 10^{-3}$ on C(100).[24] The difference in reactivity is attributed to the various extent of dimer buckling on these surfaces. Si═Si and Ge═Ge dimers can tilt out of the surface plane, shown in Fig. 1(a). In the buckling dimer, electron is transferred from the "down" atom to the "up" atom.[28] The buckling causes the dimer to behave as a dipole which can react with both electrophilic and nucleophilic functionalities and facilitates the ability of impinging molecules to find a low symmetry pathway to the final $[2+2]$ reaction product on Si(100) and Ge(100). However, there is no buckling dimer present on the clean C(100) surface, resulting in its low reactivity.[29–31] The dimer buckling is believed to be one key factor affecting the facial $[2+2]$ cycloaddition reactions on Si(100) and Ge(100) surfaces.

About 20 years ago, Chadi[32] predicted that the asymmetric configuration was energetically favorable over the symmetric dimers on Si(100). Since then a great deal of theoretical and experimental work has proven the existence of buckling dimers.[33–35] For the ground state the concept of buckling dimers is now prevailing and conclusive. At room temperature, the Si═Si dimers do not generally display asymmetry in their STM images. This may be due to the much faster dynamical flipping between the two possible buckling orientations compared to the STM measurement. At 120 K, Wolkow *et al.*[36] clearly observed a great number of tilting dimers near and away from step edges or defects,

[a)]Author to whom correspondence should be addressed. Fax: +65-779-1691; electronic mail: chmxugq@nus.edu.sg

 © 2001 American Institute of Physics

This article is copyrighted as indicated in the article. Reuse of AIP content is subject to the terms at: http://scitation.aip.org/termsconditions. Downloaded to IP: 129.237.46.99 On: Fri, 20 Nov 2015 20:22:00

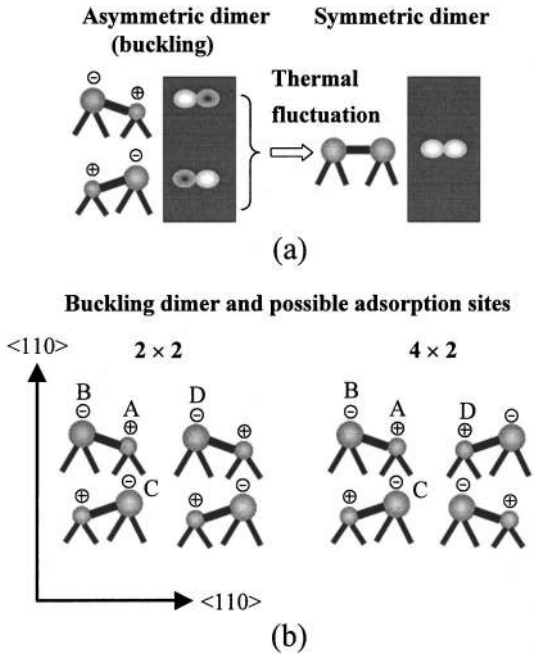

FIG. 1. The buckling dimers of the Si(100) at room temperature (a) and at a cryogenic temperature (b). A–B represents the binding site of on-top of a dimer; A–C for in-row bridging; and A–D for cross-row bridging. The symbols of ⊖ and ⊕ represent the relative charge densities of surface Si atoms.

confirming that the dimers have an asymmetric configuration at low temperature. The buckling direction observed always alternates between adjacent dimers within the same row, giving rise to "zig–zag" structures in the STM images. For this reason, the Si(100) surface mainly appears to be the combination of $p(2\times2)$ and $c(4\times2)$ reconstructions at 120 K.

It is interesting to note that the Si(100) surface at 120 K displays dipolar sites of types A–B (on-top of a dimer), A–C (in-row bridging), and A–D (cross-row bridging) for the (2×2) reconstruction, and types A–B and A–C for the (4×2) reconstruction, shown in Fig. 1(b). The three types of possible dipolar sites on the Si(100) surface at 120 K may possibly be involved in the binding of organic molecules.

To the best of our knowledge, most of the facial $[2+2]$ cycloaddition reactions on Si(100) were observed for unsaturated hydrocarbons with C═C or/and C≡C and molecules containing C═N.[37] In the case of molecules containing the polar C═O bond, the insertion of oxygen into the Si–Si was observed, resulting in molecular decomposition.[38]

In this work, the single-functionality molecule, CH_3CN containing a strongly polarized C≡N bond with a large dipole moment of 3.92 D,[39] was chosen as a template. Its adsorption behavior on Si(100) has been studied using temperature programmed desorption (TPD), x-ray photoelectron spectroscopy (XPS), high-resolution electron energy loss spectroscopy (HREELS), and density function theory (DFT) calculations. Electronic and vibrational spectra show that the acetonitrile is molecularly adsorbed on Si(100) through the C≡N group in a side-on di-σ binding mode, leaving a C═N functionality on the surface for further reaction and modification. TPD measurements reveal multiple chemisorption states corresponding to the maximum desorption temperatures of 467 K ($\beta1$) and 400 K ($\beta2$). Theoretical calculations suggest that the 1,2-dipolar cycloaddition reactions may occur at A–B and/or A–C sites for the $\beta1$ state and A–D sites for the $\beta2$.

II. EXPERIMENT

The experiments were carried out in two UHV chambers, both of which were pumped by a combination of titanium sublimation, turbo-molecular and sputter ion pumps to a base pressure less than 2×10^{-10} Torr. One chamber is equipped with high resolution electron energy loss spectrometer (HREELS, LK-2000-14R) and a quadrupole mass spectrometer (UTI-100C) for TPD. HREEL spectra were collected in a specular geometry. The electron beam with an energy of 5.0 eV impinges on the surface at an incident angle of 60° with respect to the surface normal. A typical instrumental resolution of 6–7 meV (55 cm^{-1}) was achieved. XPS studies were performed in the other chamber equipped with an x-ray source, a concentric hemispherical electron energy analyser (CLAM2, VG), and a quadrupole mass spectrometer (SRS-200). XPS spectra were acquired using Al $K\alpha$ radiation ($h\nu=1486.6$ eV) and 20 eV pass energy. For XPS the binding energy (BE) scale is referenced to the peak maximum of the Si $2p$ line (99.3 eV) (Ref. 40) of the clean Si(100) substrate with a full width at half maximum (FWHM) of less than 1.2 eV.

The Si(100) samples were cut from *p*-type *B*-doped Si wafers (99.999%, 1–30 Ω cm) purchased from Goodfellow. Two pieces of Si(100) single crystals of the same dimension ($18\times10\times0.38$ mm^3) were deposited with a thin Ta layer (~2000Å thick) on their unpolished backsides for homogeneous heating and cooling. The Si(100) samples were mounted using the following procedure. A piece of Ta foil (0.025 mm thick, Goodfellow) was sandwiched between the Ta-covered backsides of the two silicon samples to act as a heater. The samples were clamped together using two clips for fixation. The sandwiched Ta foil was then spot-welded to two Ta rods connected to the Cu feedthroughs of the manipulator. A 0.003 in. W–5%Re/W–26%Re thermocouple was attached to the center of one silicon sample using high temperature ceramic adhesive (Aremco 516) for temperature measurement. Such mounted silicon samples can be resistively heated to 1400 K by resistive heating and conductively cooled to 110 K using liquid nitrogen within 15 min. The temperature distribution across the sample was within ±10 K at 1000 K as verified by an infrared pyrometer.

The silicon samples were thoroughly degassed at 900 K in the UHV chamber until a pressure less than 3×10^{-10} Torr was achieved. Surface contaminants, such as silicon carbide and silicon nitride were removed by repeated cycles of Ar^+ (500 eV, 10 mA cm^{-1}) bombardment and subsequent annealing to 1300 K. Surface cleanliness was confirmed by XPS and HREELS. Acetonitrile CH_3CN (99.5+%,) and acetonitrile-d_3 CD_3CN (99.95%) were purchased from Aldrich and purified by freeze–pump–thaw cycles prior to use. Dosing was conducted by backfilling the chamber through a variable leak-valve and exposures were calculated without ion gauge sensitivity calibration.

This article is copyrighted as indicated in the article. Reuse of AIP content is subject to the terms at: http://scitation.aip.org/termsconditions. Downloaded to IP: 129.237.46.99 On: Fri, 20 Nov 2015 20:22:00

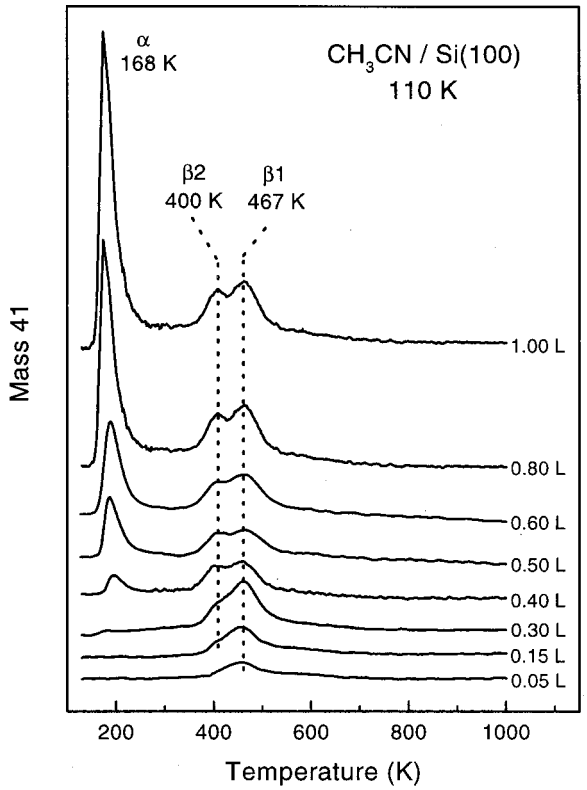

FIG. 2. TPD spectra of $C_2H_3N^+$ ($m/e=41$) from Si(100) as a function of acetonitrile exposure at 110 K. A heating rate of 2 K s^{-1} was employed.

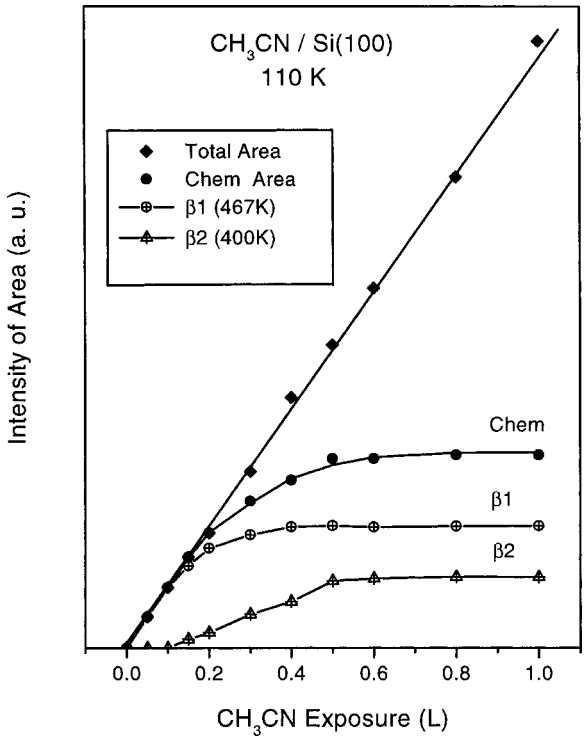

FIG. 3. The desorption peak area as a function of CH_3CN exposure.

III. RESULTS

A. Temperature programmed desorption

TPD spectra for the Si(100) surface exposed to an increasing amount of CH_3CN at 110 K are shown in Fig. 2. CH_3CN was the only desorption product detected. For small exposures of $\leqslant$0.1 L (1 Langmuir$=1\times10^{-6}$ Torr s), a single desorption peak ($\beta1$) is observed at 467 K. With increasing exposures, a new desorption feature, $\beta2$ appears at 400 K along with the $\beta1$ peak. In addition, a low temperature peak (α) at 168 K becomes noticeable at 0.3 L and dominates the spectrum at high exposures. We assign $\beta1$ and $\beta2$ to chemisorbed CH_3CN and α to physisorbed CH_3CN. Figure 3 shows the integrated peak areas of the $\beta1$ and $\beta2$ peaks, the chemisorbed layer ($\beta1+\beta2$), and the total adsorption ($\alpha+\beta1+\beta2$) as a function of the CH_3CN exposure. Figure 3 indicates that the Si(100) surface is nearly saturated by chemisorbed CH_3CN for 0.4–0.5 L at 110 K and that the area of the $\beta1$ peak is ~60% of the saturated chemisorbed layer. The figure also shows that physisorption occurs before the saturation of chemisorbed layer, indicating the island growth mode. The linear dependence of the total integrated area as a function of exposure suggests the unitary sticking probability for acetonitrile adsorbed on Si(100) at 110 K.

B. X-ray photoelectron spectroscopy

XPS of the C 1s and N 1s regions were taken as a function of exposure and the results are shown in Fig. 4. For monolayer and submonolayer coverages, the C 1s and N 1s peaks were observed at 284.5 and 397.2 eV, respectively. A small intensity near 288 eV is noticed in the C 1s spectrum of 0.20 L, attributable to the noise, not the photoemission peak as its FWHM (<0.5 eV) is even much smaller than that (~1 eV) of our x-ray source. When the physisorption layer was formed, new peaks appeared at 287.0 (C 1s) and 400.2

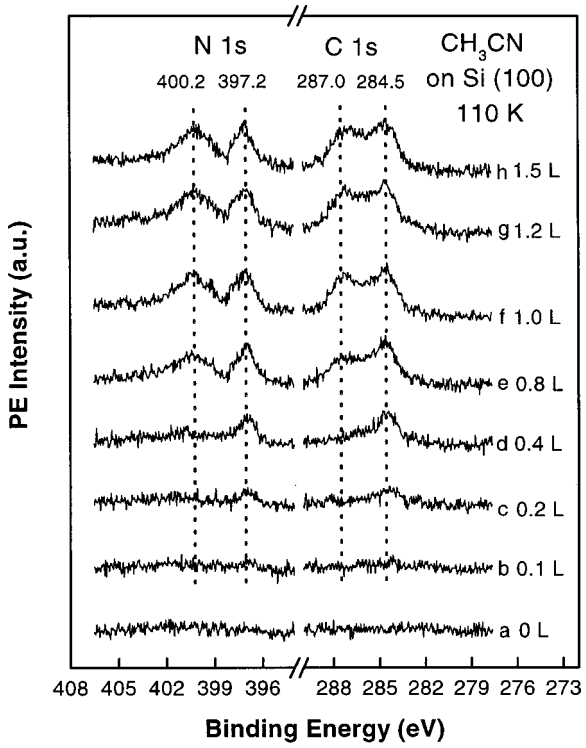

FIG. 4. The C 1s and N 1s binding energies (eV) of CH_3CN adsorbed on Si(100) at 110 K as a function of exposure.

This article is copyrighted as indicated in the article. Reuse of AIP content is subject to the terms at: http://scitation.aip.org/termsconditions. Downloaded to IP: 129.237.46.99 On: Fri, 20 Nov 2015 20:22:00

TABLE I. C 1*s* and N 1*s* BEs (eV) of CH_3CN adsorbed on different substrates.

Sample	Multilayer		Monolayer		BE shifts (eV)		Binding mode	References
	C 1*s*	N 1*s*	C 1*s*	N 1*s*	C 1*s*	N 1*s*		
Pt(111)	286.9	400.1	284.6	397.2	2.3	2.9	Side-on	43
Ni(111)	287.0	400.2	284.5	397.7	2.5	2.5	Side-on	44, 45
Cu(100)	287.3	400.3	286.6	399.7	0.7	0.6	End-on	42
Ni film	287.0	400.2	284.5	397.7	2.5	2.5	Side-on	46
Pd film	287.0	400.2	284.5	397.5	2.5	2.7	Side-on	46
Si(100)	287.0	400.2	284.5	397.2	2.5	3.0	Side-on	This work

eV (N 1*s*). With a large exposure, the monolayer state was completely attenuated, leaving only the C 1*s* and N 1*s* peaks (not shown) of the thick physisorbed multilayer CH_3CN. The chemisorbed acetonitrile monolayer was obtained by annealing the acetonitrile-exposed Si(100) surface to 250 K to drive away physisorbed molecules and only leave chemisorbed species on the Si surface. The collected XPS spectra show a single set of C 1*s* and N 1*s* peaks at 284.5 and 397.2 eV, respectively, which is characteristic of chemisorbed CH_3CN on Si(100). The C 1*s* peak corresponds to C atoms of both the CH_3 and CN groups. The fact that only one C 1*s* peak is observed in either physisorbed or chemisorbed state is consistent with CH_3CN adsorption on other substrates.[41–45] This may be related to the nature of the molecules. In the gas phase, XPS of acetonitrile[46] shows that the C 1*s* peaks for C (CH_3) and C (CN) atoms are separated by less than 0.6 eV.

If CH_3CN was weakly chemisorbed on Si(100) through an end-on binding, we would expect little perturbation to the molecular electronic structure and only slight shift, from the physisorbed multilayer BEs, particularly for C 1*s*. For example, for acetonitrile adsorbed on Cu(100) with an end-on binding mode, the C 1*s* peak only shows a small chemical shift of 0.7 eV as listed in Table I.[42] However, our experimental results show that both C 1*s* and N 1*s* peaks of chemisorbed CH_3CN display large chemical shifts of 2.5 and 3.0 eV, respectively, from those of the physisorbed multilayer, which suggests that CH_3CN binds to Si(100) through both C and N atoms of the CN group. Table I also shows that the characteristic C 1*s* and N 1*s* binding energies for chemisorbed CH_3CN on Si(100) are very similar to those for CH_3CN chemisorbed on other substrates with a side-on binding mode.[43–46]

C. High-resolution electronic energy loss spectroscopy

Figure 5 presents the HREEL spectra as a function of CH_3CN exposure on Si(100) at 110 K. At low exposures, obvious loss features are identified at 412, 695, 835, 952, 1065, 1397, 1464, 2970, 3012 cm^{-1}. In addition, a noticeable loss feature around 1550–1650 cm^{-1} appears as a shoulder on the right-hand side of the broad peak at 1464 cm^{-1}. With increasing CH_3CN exposure, the disappearance of the energy loss around 1550–1650 cm^{-1} (the shoulder on the right-hand side of the main peak at 1464 cm^{-1}), whose assignment will be discussed later, and the appearance of a new energy loss peak at 2218 cm^{-1} corresponding to the stretching mode of C≡N bond, can be unambiguously resolved. The characteristics of chemisorbed CH_3CN are gradually screened by the subsequent physisorbed multilayers. After dosing >0.40 L of CH_3CN, these energy loss features of physisorbed multilayers demonstrated in Fig. 5 and Table II agree well with the vibrational frequencies of gas phase acetonitrile within 20 cm^{-1}. The detailed assignments for physisorbed CH_3CN together with the IR data[47] of gas-phase CH_3CN are summarized in Table II.

As shown in Fig. 5, there is an obvious shoulder around 1550–1650 cm^{-1} which is close to the CH_3 bending mode and is possibly attributable to the stretching mode of the C═N bond in the chemisorbed molecules. In order to confirm its assignment, saturated chemisorbed monolayers of CH_3CN and CD_3CN were prepared through annealing the sample pre-exposed to 1.0 L CH_3CN or CD_3CN to 250 K to drive away all physisorbed multilayers and their HREEL

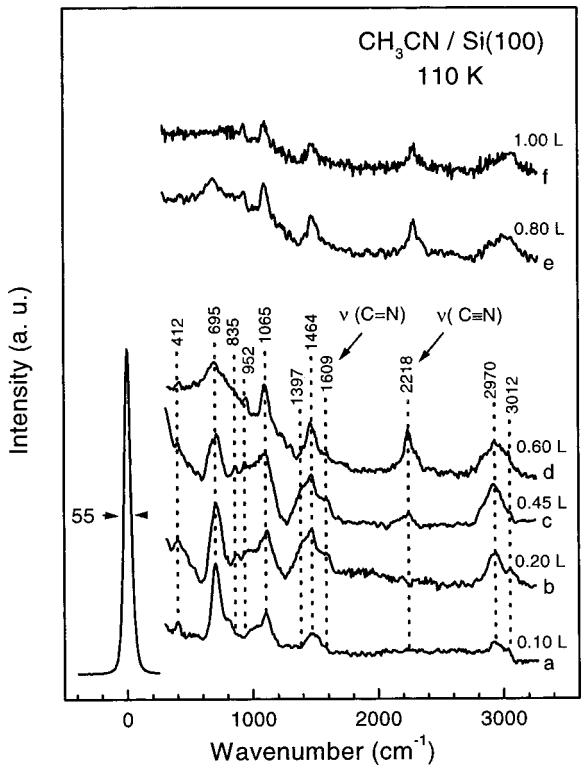

FIG. 5. HREEL spectra as a function of CH_3CN exposure to Si(100) at 110 K.

This article is copyrighted as indicated in the article. Reuse of AIP content is subject to the terms at: http://scitation.aip.org/termsconditions. Downloaded to IP: 129.237.46.99 On: Fri, 20 Nov 2015 20:22:00

TABLE II. Assignment of vibrational frequencies (cm^{-1}) for CH_3CN adsorbed on Si(100) at 110 K.

Vibrational mode	Description	CH_3CN gas phase[a]	Physisorbed CH_3CN on Si(100)	Chemisorbed CH_3CN on Si(100)	Chemisorbed CH_3CN on Pt(111)[b]	Chemisorbed CD_3CN on Si(100)	Chemisorbed CD_3CN on Pt(111)[b]
δ (C–C–N)	CCN bend	361	⋯	412	605	398	580
ν (Si–C)	SiC stretch	⋯	⋯	695	⋯	650	⋯
ν (Si–N)	SiN stretch	⋯	⋯	835	⋯	848	⋯
ν (C–C)	CC stretch	920	915	952	950	942	930
$\rho_r(CH_3)$	Methyl rock	1041	1026	1065	1060	848	850
$\sigma_s(CH_3)$	Methyl sym. bend	1389	1392	1397	1374		
						1124	1100
$\sigma_d(CH_3)$	Methyl deg. bend	1454	1434	1464	1435		
ν(C═N)	C═N stretch	⋯	⋯	1603	1615	1595	1625
ν(C≡N)	C≡N stretch	2268	2218	⋯	⋯	⋯	⋯
ν_s(CH)	CH_3 sym. stretch	2954		2970	2960		2120
			3005			2210	
ν_d(CH)	CH_3 deg. stretch	3009		3012	3012		2280

[a]Reference 47.
[b]Reference 43.

spectra are shown in Fig. 6. For chemisorbed CH_3CN, losses at 412, 695, 835, 952, 1065, 1415, 1603, 2970, and 3012 cm^{-1} are readily identified; losses at 398, 650, 848, 952, 1124, 1595, and 2210 cm^{-1} are clearly observed for the chemisorbed CD_3CN. Table II lists their detailed assignments. The most important features to be noted in Fig. 6(a) are (1) all vibrational modes related to C–H bonds display obvious red shifts; in particular, the methyl bending mode shifts from 1397 and 1464 cm^{-1}($-CH_3$) to 1124 cm^{-1}($-CD_3$); (2) the shoulder around 1550–1650 cm^{-1} [Fig. 6(b)] remains nearly unshifted and appears as an isolated peak at 1595 cm^{-1} in the chemisorbed CD_3CN. Therefore, the shoulder around 1550–1650 cm^{-1} of chemisorbed CH_3CN [Fig. 6(b)] and the isolated peak at 1595 cm^{-1} of CD_3CN [Fig. 6(a)] are assigned to the stretching mode of the C═N bond in chemisorbed acetonitrile. This assignment clearly demonstrates the rehybridization of both carbon and nitrogen atoms of the CN group from *sp* to sp^2 after chemisorption. The similar HREEL spectra, particularly for the vibration around 1600 cm^{-1}, were reported for chemisorbed CH_3CN on Pt(111) with a side-on di-σ binding mode.[43] Moreover, the assignment of the shoulder at 1603 cm^{-1} as the C═N stretching mode also rules out the possibility of CN group binding to Si(100) through a side-on tetra-σ binding mode.

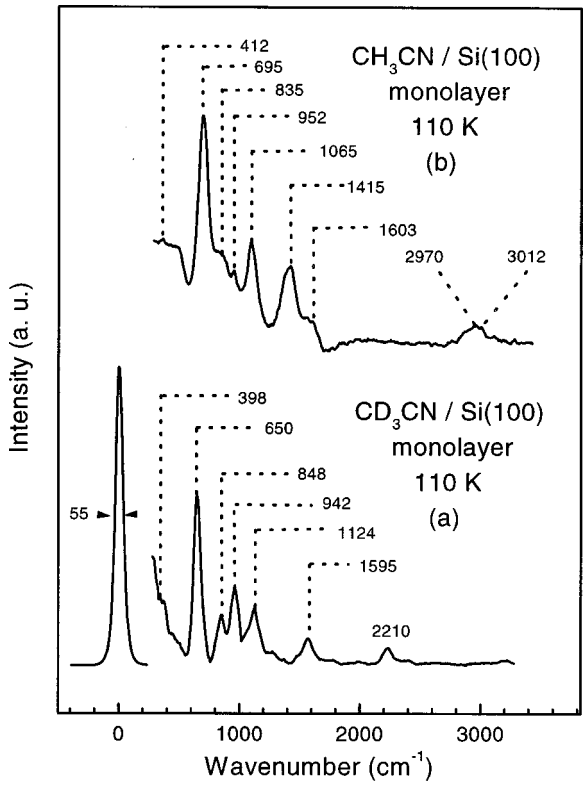

FIG. 6. HREEL spectra of chemisorbed (a) CD_3CN and (b) CH_3CN.

In order to study the thermal evolution of chemisorbed CH_3CN on Si(100), the sample was pre-exposed to 1.0 L CH_3CN at 110 K, followed by annealing to 250 K. This procedure drives off all the physisorbed CH_3CN, leaving a chemisorbed monolayer on the surface, which shows a HREEL spectrum similar to that of Fig. 6(b). As shown in Fig. 7, upon annealing the sample to 420 K, losses at 695, 835, 952, 1065, 1464, 1603, and 2992 cm^{-1} can be resolved, which are the same feature as that observed at 250 K. However, peak intensities are obviously reduced due to the molecular desorption around 400 K. No peaks located between 2000–2150 cm^{-1} corresponding to ν(Si–H), can be found, which further confirms the nondissociative nature of CH_3CN adsorption on Si(100). At 550 K, the vibrational characteristics of chemisorbed CH_3CN completely disappear, consistent

This article is copyrighted as indicated in the article. Reuse of AIP content is subject to the terms at: http://scitation.aip.org/termsconditions. Downloaded to IP: 129.237.46.99 On: Fri, 20 Nov 2015 20:22:00

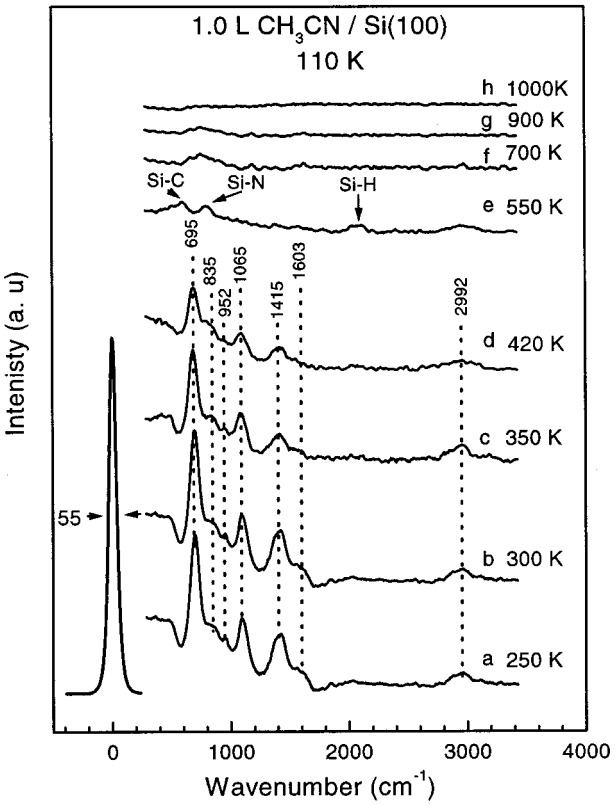

FIG. 7. HREEL spectra obtained from Si(100) exposed to 1.0 L CH_3CN at 110 K and then annealed to corresponding temperatures.

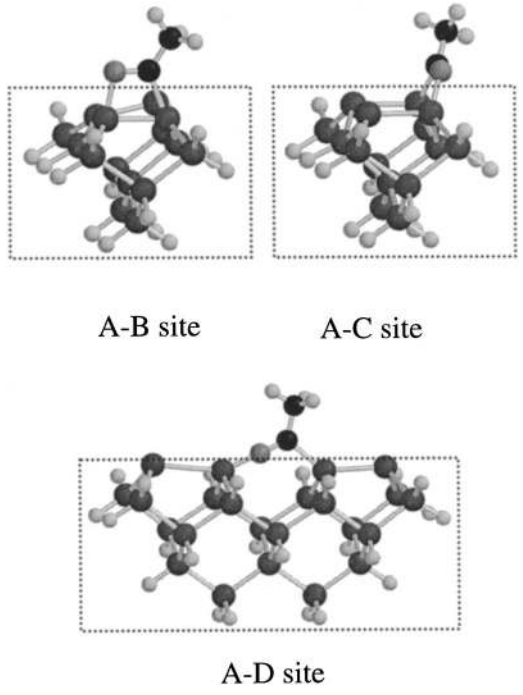

FIG. 8. Cluster models of CH_3CN on Si(100) optimized by DFT calculations.

with molecular desorption at 400 and 467 K observed by TPD. However, a small amount of CH_3CN does decompose, as evidenced by the appearance of Si–C, Si–N, and Si–H loss features. The dissociation of trace amount of CH_3CN is possibly attributable to those molecules adsorbed at defect sites. These features eventually disappear at 1000 K, plausibly due to C and N diffusion into the bulk phase.

IV. DISCUSSION

TPD spectra for CH_3CN chemisorbed on Si(100) show two desorption peaks at 400 ($\beta 2$) and 467 K ($\beta 1$), indicating the existence of multiple chemisorption states. The activation energies of desorption for the $\beta 1$ and $\beta 2$ peaks are estimated to be 29.8 and 24.6 kcal mol^{-1}, respectively, using the Redhead formula[48] and assuming a first-order desorption behavior and pre-exponential factor of 10^{13} s^{-1}.

The evolution of the area intensities of the $\beta 1$ and $\beta 2$ peaks from the chemisorbed layer with CH_3CN exposure (Fig. 3) indicates that the $\beta 1$ peak contributes about 60% of the saturated chemisorbed layer and 40% from the $\beta 2$ peak. The proportions of the $\beta 1$ and $\beta 2$ states are too high to be simply attributed to chemisorption at the defect sites ($\sim$5%).[49] There are two possible well-established chemisorption modes for CH_3CN on different single crystal surfaces.[42–46] For the end-on binding mode, as is the case of CH_3CN chemisorbed on Cu(100), the N atom of the CN group weakly interacts with the surface through the N lone pair electrons and a small 0.7 eV BE shift is observed for the C 1*s* core-level.[42] For the side-on di-σ binding mode observed from CH_3CN chemisorbed on Ni(111) and Pt(111), the binding energies of both C 1*s* and N 1*s* core levels display large chemical shifts of about 2.3–2.9 eV.[43–45] In the present CH_3CN adsorbed on Si(100), comparison of the C 1*s* and N 1*s* BEs between physisorbed and chemisorbed layers shows significant chemical shifts of 2.5 eV (C 1*s*) and 3.0 eV (N 1*s*). This result suggests that CH_3CN binds to Si(100) in a side-on binding mode. Further, the appearance of loss peak at 1603 cm^{-1} for chemisorbed CH_3CN (1595 cm^{-1} for chemisorbed CD_3CN) attributable to the C═N bond stretching mode is a conclusive proof of di-σ side-on binding.

For the side-on di-σ binding mode, TPD measurements show the presence of two desorption peaks, $\beta 1$ and $\beta 2$ possibly corresponding to desorption from two or more adsorption sites as shown in Fig. 1(b). In order to assign them, DFT calculations using SPARTAN 5.1.3 (density functional theory *p*BP with a basis set DN*)[50,51] were performed to obtain binding energies at the different adsorption sites A–B, A–C, and A–D. Based on these three possible adsorption sites, two clusters were built to model these adsorbed products as shown in Fig. 8. Cluster I, corresponding to adsorption sites A–B (on top of one dimer) and A–C (in-row bridging), is a $Si_{15}H_{16}$ cluster which has two exposed Si═Si dimers in a dimer row. Cluster II, $Si_{23}H_{24}$, corresponding to adsorption site A–D (cross-row bridging), is an extension of cluster I to include two surface dimers in two adjacent dimer rows. In these two clusters, Si atoms at the cluster edges were terminated with H atoms to provide complete coordination for all atoms except those forming the surface dimers. Molecular binding energies were obtained by first placing the CH_3CN molecule at an appropriate binding site on the model cluster, and then allowing all atomic positions to adjust to find local minimum in energy. The energies of the optimized free clus-

This article is copyrighted as indicated in the article. Reuse of AIP content is subject to the terms at: http://scitation.aip.org/termsconditions. Downloaded to IP: 129.237.46.99 On: Fri, 20 Nov 2015 20:22:00

ter and the optimized free molecule were then subtracted from the total energy of the corresponding product to yield a net binding energy. The calculated binding energy for the A–B site, 31.6 kcal mol^{-1}, agrees well with the desorption energy (29.8 kcal mol^{-1}) of the $\beta 1$ peak from TPD measurements. Interestingly, the calculated value for the A–C site, 30.3 kcal mol^{-1}, is very close to that of the A–B site. Thus, the $\beta 1$ may be related to acetonitrile binding to A–B and/or A–C sites. This possibly results from the existence of similar dipole reactive sites at Si(A)–Si(B) and Si(A)–Si(C) due to the alternative buckling direction of neighboring dimers in the same dimer row.[35] The small difference in their binding energies may result from the slight change in distances between Si(A)–Si(B) and Si(A)–Si(C). On the other hand, the calculated binding energy of 22.1 kcal mol^{-1} for the A–D site is close to the experimental value (24.6 kcal mol^{-1}) from TPD measurements for the $\beta 2$ peak. Hence, we attribute the $\beta 2$ peak to the chemisorption occurring at A–D sites. Considering the larger distance of 5.8 Å for Si(A)–Si(D) compared to 2.3 Å for Si(A)–Si(B), adsorption at A–D sites is expected to be significantly weaker. A similar comparison was made for benzene binding on Si(111)-7×7 and excellent agreement was achieved.[52,53] Therefore, on the basis of DFT calculations, it seems reasonable to assign the $\beta 1$ desorption peak to the molecules adsorbed on the sites of A–B and/or A–C, and the $\beta 2$ to the desorption from the A–D adsorption site.

V. CONCLUSIONS

Both XPS and HREELS experimental evidences unambiguously demonstrates that acetonitrile is covalently bonded on Si(100) with a side-on di-σ binding mode through a 1,2-dipolar cycloaddition mechanism. TPD measurements uncover two desorption peaks, $\beta 1$ and $\beta 2$, at 467 and 400 K, respectively. DFT calculations indicate that the $\beta 1$ peak possibly corresponds to acetonitrile adsorbed on top of a dimer and/or in an in-row bridging mode, and the $\beta 2$ is possibly related to acetonitrile adsorbed at cross-row bridging sites. The surface intermediate formed by acetonitrile modification containing an imine C═N bond can be a useful interfacial precursor for further modifying and functionizing Si surfaces.

[1] J. T. Yates, Jr., Science **279**, 335 (1998).
[2] R. E. Schlier and H. E. Farnsworth, J. Chem. Phys. **30**, 917 (1959).
[3] R. M. Tromp, R. J. Hamers, and J. E. Demuth, Phys. Rev. Lett. **55**, 1303 (1985).
[4] R. J. Hamers, R. M. Tromp, and J. E. Demuth, Phys. Rev. B **34**, 5343 (1986).
[5] R. J. Hamers, R. M. Tromp, and J. E. Demuth, Surf. Sci. **181**, 346 (1986).
[6] J. Yoshinobu, H. Tsuda, and M. Nishijima, J. Chem. Phys. **87**, 7332 (1987).
[7] L. Clemen, R. M. Wallace, P. A. Taylor, M. J. Dresser, W. J. Choyke, W. H. Weinberg, and J. T. Yastes, Jr., Surf. Sci. **268**, 205 (1992).
[8] B. I. Craig and P. V. Smith, Surf. Sci. **285**, 295 (1993).
[9] C. C. Cheng, R. M. Wallace, P. A. Taylor, W. J. Choyke, and J. T. Yates, Jr., J. Appl. Phys. **67**, 3693 (1990).
[10] W. Widdra, C. Huang, S. I. Yi, and W. H. Weinberg, J. Chem. Phys. **105**, 5605 (1996).
[11] C. Huang, W. Widdra, and W. H. Weinberg, Surf. Sci. **315**, L953 (1994).
[12] Y. Imamura, Y. Morikawa, T. Yamasaki, and H. Nakatsuji, Surf. Sci. **341**, L1091 (1994).
[13] A. J. Fisher, P. E. Blocjl, and G. A. D. Briggs, Surf. Sci. **374**, 298 (1997).
[14] M. J. Bozack, P. A. Taylor, W. J. Choke, and J. T. Yates, Jr., Surf. Sci. **177**, L933 (1986).
[15] R. J. Hamers, J. S. Hovis, S. Lee, H. Liu, and J. Shan, J. Phys. Chem. B **101**, 1489 (1997).
[16] J. S. Hovis, H. Liu, and R. J. Hamers, J. Phys. Chem. B **102**, 6873 (1997).
[17] J. S. Hovis and R. J. Hamers, J. Phys. Chem. B **101**, 9581 (1997).
[18] J. S. Hovis and R. J. Hamers, J. Phys. Chem. B **102**, 687 (1998).
[19] J. S. Hovis, S. Lee, H. Liu, and R. J. Hamers, J. Vac. Sci. Technol. B **15**, 1153 (1997).
[20] H. Liu and R. J. Hamers, Surf. Sci. **416**, 354 (1998).
[21] C. Huang, W. Widdra, X. S. Wang, and W. H. Weinberg, J. Vac. Sci. Technol. A **11**, 2250 (1993).
[22] H. Liu and R. J. Hamers, J. Am. Chem. Soc. **119**, 7593 (1997).
[23] R. B. Woodward and R. Hoffmann, *The Conversion of Orbital Symmetry* (Academic, New York, 1970).
[24] J. S. Hovis, R. J. Hamers, M. P. D'Evelyn, J. N. Russell, Jr., and J. E. Butler, J. Am. Chem. Soc. **122**, 732 (2000).
[25] R. J. Hamers, J. S. Hovis, C. M. Greenlief, and D. F. Padowitz, Jpn. J. Appl. Phys. **38**, 3879 (1999).
[26] P. Lai, A. V. Teplyakov, Y. A. Noah, M. J. Kong, G. T. Wang, and S. F. Bent, J. Chem. Phys. **110**, 10545 (1999).
[27] A. V. Teplyakov, P. Lal, Y. A. Noah, and S. F. Bent, J. Am. Chem. Soc. **120**, 7377 (1998).
[28] Q. Liu and R. Hoffman, J. Am. Chem. Soc. **117**, 4082 (1995).
[29] T. I. Hukka, T. A. Pakkanen, and M. P. D'Evelyn, J. Phys. Chem. **98**, 12420 (1994).
[30] T. W. Mercer and P. E. Pehrsson, Surf. Sci. **399**, L327 (1998).
[31] Y. L. Kuang, Y. F. Wang, N. Lee, T. Badzian, and T. T. Tsong, Appl. Phys. Lett. **67**, 3721 (1995).
[32] D. J. Chadi, Phys. Rev. Lett. **43**, 43 (1979).
[33] R. I. G. Uhrberg, G. V. Hansson, J. M. Nicholls, and S. A. Flodstrom, Phys. Rev. B **24**, 4684 (1981).
[34] R. J. Hamers and U. K. Kohler, J. Vac. Sci. Technol. A **7**, 2854 (1989).
[35] R. J. Hamers and Y. J. Wang, Chem. Rev. **96**, 1261 (1996).
[36] R. A. Wolkow, Phys. Rev. Lett. **68**, 2636 (1992).
[37] M. D. Ellsion and R. J. Hamers, J. Phys. Chem. B **103**, 6243 (1999).
[38] J. L. Armstrong, E. D. Pylant, and J. M. Whites, J. Vac. Sci. Technol. A **16**, 123 (1998).
[39] *CRC Handbook of Chemistry and Physics*, 68th ed. (CRC, Boca Raton, FL, 1987).
[40] *Handbook of X-Ray Photoelectron Spectroscopy* (Perkin–Elmer, Minnesota, 1992).
[41] B. A. Sexton and A. E. Hughes, Surf. Sci. **140**, 227 (1984).
[42] B. A. Sexton and N. R. Avery, Surf. Sci. **129**, 21 (1983).
[43] C. M. Friend, E. L. Muetterties, and J. L. Gland, J. Phys. Chem. **85**, 3256 (1981).
[44] K. Kishi, K. Chinomi, Y. Inoue, and S. Ikeda, J. Catal. **60**, 228 (1979).
[45] K. Kishi and S. Ikeda, Surf. Sci. **107**, 405 (1981).
[46] T. Fujikawa, T. Ohta, and H. Kuroda, Bull. Chem. Soc. Jpn. **49**, 1486 (1976).
[47] J. E. D. Davies, J. Mol. Struct. **9**, 483 (1971).
[48] P. A. Redhead, Vacuum **12**, 203 (1962).
[49] Z. C. Dong, T. Yakabe, D. Fujita, Q. D. Jiang, and H. Nejo, Surf. Sci. **380**, 23 (1997).
[50] SPARTAN 5.1.3, Wavefunction, Inc., Irvine, CA, 1998.
[51] W. J. Hehre, J. Yu, and P. E. Klunzinger, A Guide to Molecular Mechanics and Molecular Orbital Calculations in SPARTAN, Wavefunction, Inc., Irvine, CA, 1997.
[52] Z. H. Wang, Y. Cao, and G. Q. Xu, Chem. Phys. Lett. **338**, 7 (2001).
[53] Y. Cao, X. M. Wei, W. S. Chin, Y. H. Lai, J. F. Deng, S. L. Bernasek, and G. Q. Xu, J. Phys. Chem. B **103**, 5698 (1999).

This article is copyrighted as indicated in the article. Reuse of AIP content is subject to the terms at: http://scitation.aip.org/termsconditions. Downloaded to IP: 129.237.46.99 On: Fri, 20 Nov 2015 20:22:00